ACS OMEGA

Article

Cite This: ACS Omega 2018, 3, 10243−10249

http://pubs.acs.org/journal/acsodf

Bimetallic CoMoS Composite Anchored to Biocarbon Fibers as a High-Capacity Anode for Li-Ion Batteries

Noemi Dominguez,[†] Brenda Torres,[‡,§] Luis A. Barrera,[§] Julio E. Rincon,[†] Yirong Lin,[∥] Russell R. Chianelli,[‡,§] Md. Ariful Ahsan,[§] and Juan C. Noveron*[,§]

[†]Department of Metallurgical, Materials and Biomedical Engineering, [‡]Materials Research and Technology Institute, [§]Department of Chemistry, and [∥]Department of Mechanical Engineering, The University of Texas at El Paso, El Paso, Texas 79968, United States

Supporting Information

ABSTRACT: Our work reports the hydrothermal synthesis of a bimetallic composite CoMoS, followed by the addition of cellulose fibers and its subsequent carbonization under Ar atmosphere (CoMoS@C). For comparison, CoMoS was heat-treated under the same conditions and referred as bare-CoMoS. X-ray diffraction analysis indicates that CoMoS@C composite matches with the $CoMoS_4$ phase with additional peaks corresponding to MoO_3 and $CoMoO_4$ phases, which probably arise from air exposure during the carbonization process. Scanning electron microscopy images of CoMoS@C exhibit how the CoMoS material is anchored to the surface of carbonized cellulose fibers. As anode material, CoMoS@C shows a superior performance than bare-CoMoS. The CoMoS@C composite presents an initial high discharge capacity of ∼1164 mA h/g and retains a high specific discharge capacity of ∼715 mA h/g after 200 cycles at a current density of 500 mA/g compared to that of bare-CoMoS of 102 mA h/g. The high specific capacity and good cycling stability could be attributed to the synergistic effects of CoMoS and carbonized cellulose fibers. The use of biomass in the anode material represents a very easy and cost-effective way to improve the electrochemical Li-ion battery performance.

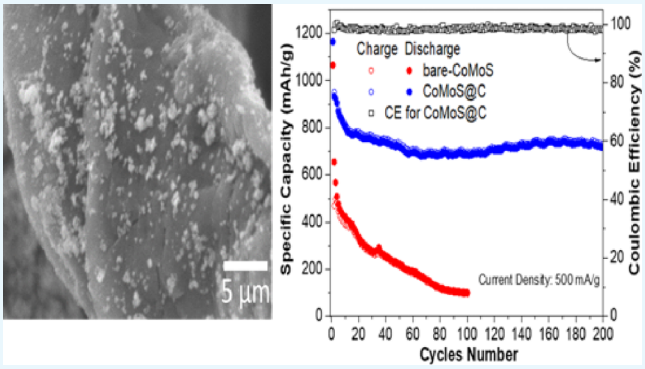

1. INTRODUCTION

To date, Li-ion batteries (LIBs) have been widely utilized for portable electronic devices because of their promising properties, including high energy density, long cycle lifetime, and low self-discharge.[1] However, to meet nowadays the energy demands for high-power applications, as in the case of electric vehicles and smart grid systems, it is essential to find new anode materials with higher rate capacity, longer cycling lifetime, and higher capacity to that of graphite (372 mA g^{-1}),[2] the anode material currently used for commercially available LIBs.

Recently, transition metal sulfides have reached great attention as anode materials for LIBs because of their high theoretical capacity.[3−5] For example, molybdenum sulfide (MoS_2) has a theoretical capacity value of 670 mA h/g[6,7] (almost twice that of graphite). Additionally, MoS_2 holds a layer structure that enables easy intercalation of Li ions within the (002) planes, hence proving a fast diffusion of ions during electrochemical processes.[8,9] However, this material suffers from low electric conductivity as well as poor cycling stability because of its inherent high volume change during the charging/discharging steps.[8] On the other hand, cobalt sulfides with different compositions (CoS_2, CoS, and Co_9S_8) have shown encouraging results as anode materials for LIBs.[10−14] Moreover, cobalt sulfides possess higher electrical conductivity compared to other metal sulfides[15,16] but also suffers from rapid capacity decay.[17]

Composites of MoS_2 and cobalt sulfides, as well as CoMoS phases, have been investigated for other applications, including, catalysis in hydrodeoxygenation,[18,19] hydrodesulfurization,[18,20] and hydrogen evolution reaction,[21−24] among others. However, only a few reports of the combination of molybdenum and cobalt sulfides for its application in LIBs have been reported.[9,25] The combination of these two metal (Mo and Co) sulfides can offer synergistic advantages over single systems as it has been reported for other bimetallic sulfides for sodium-ion battery applications.[26,27] Additionally, to improve the electrochemical performance of LIBs, transition metal compounds have been combined with carbon-based materials such as reduced graphene[28,29] and carbon nanotubes,[30,31] both of which are expensive materials and require elaborate methods for fabrication. On the other hand, promising results for LIB applications have been achieved from the combination of transition metal compounds and biomass-derived carbon.[32−34] The use of biomass represents an

Received: April 4, 2018
Accepted: July 20, 2018
Published: August 30, 2018

DOI: 10.1021/acsomega.8b00654
ACS Omega 2018, 3, 10243−10249

easy and low-cost alternative to enhance the electrochemical performance of LIBs.

Here, we present the synthesis of a bimetallic CoMoS composite by the hydrothermal method and the addition of cellulose fibers as a carbon source, followed by carbonization under argon atmosphere (CoMoS@C). The CoMoS@C composite was characterized by X-ray diffraction (XRD), scanning electron microscopy (SEM), energy-dispersive spectroscopy (EDS), thermogravimetric analysis (TGA), and transmission electron microscopy (TEM). To investigate its electrochemical properties as anode material for LIBs, galvanostatic, cyclic voltammetry (CV), and electrochemical impedance spectroscopy measurements (EIS) were performed. The addition of carbon significantly enhanced the cycling stability and retained a high specific capacity of ∼715 mA h/g after 200 cycles at a rate of 500 mA h/g compared to bare-CoMoS which retained ∼102 mA h/g after 100 cycles.

2. RESULTS AND DISCUSSION

The crystal structures of CoMoS (before heat treatment), bare-CoMoS, and CoMoS@C were characterized by XRD (Figure 1b–d). It can be seen that most of the peaks from the three

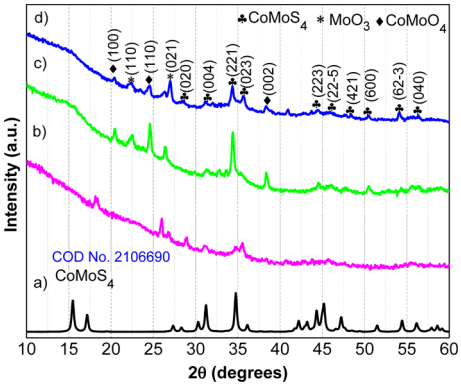

Figure 1. XRD diffractograms of (a) standard spectrum for $CoMoS_4$, (b) CoMoS (before heat treatment), (c) bare-CoMoS (after heat treatment at 400 °C for 1 h under Ar), and (d) CoMoS@C.

samples match with the $CoMoS_4$ phase registered in the COD (Crystallographic Open Database)[36] no. 2106690 (Figure 1a). However, bare-CoMoS and CoMoS@C X-ray spectrums (Figure 1c,d) show additional peaks corresponding to MoO_3 and $CoMoO_4$ phases with COD numbers 1011043 and 7205001, respectively. We can see that most of the peaks corresponding to the oxide phases appeared after the compounds were subjected to heat treatment at 400 °C (comparison of Figure 1b,c,d). Therefore, these peaks were most likely formed by the accidental air exposure while the carbonization process was carried out. Additionally, bare-CoMoS and CoMoS@C present very similar XRD patterns. Nevertheless, it can be observed that bare-CoMoS displays sharper peaks than those found in CoMoS@C, which shows broader peaks possibly because of the poorly crystalline nature of the carbonized cellulose fibers (Figure S1).

The SEM micrographs of three samples are presented in Figure 2a,b,d,e. From Figure 2a, we can observe micron-sized particle clusters for the bare-CoMoS sample. An elongated ribbonlike morphology can be observed for cellulose fibers carbonized at 400 °C for 1 h with diameter sizes ranging from 5 to 22 μm and an average size of ∼10 μm (Figure 2b). For sample CoMoS@C (Figure 2d), it is observed that some carbonized cellulose fibers (with less than 10 μm in diameter size) are decorated with CoMoS particle clusters with less than one micron in size. Larger CoMoS particle clusters standing apart from the fibers can also be seen. The SEM image (Figure 2e) of an individual microfiber at larger magnification shows that the particle clusters anchored to its surface have diameter sizes ranging from 0.3 to 2 μm with a seemingly uniform particle distribution along the fiber. A more detailed perspective of the morphology can be appreciated in the TEM images of bare-CoMoS and CoMoS@C (Figure 2c,f, respectively). Aggregates of nanosheets can be observed for both materials with no significant differences between the two samples.

To obtain information about the chemical composition of the samples, EDS analysis was performed. Figure 3a shows the SEM selected area of CoMoS@C for EDS analysis. As can be seen, the selected area is composed of both CoMoS particles and carbon fibers. The EDS spectrum of CoMoS@C (Figure 3f) confirms that this sample is composed of Mo, S, Co, and C elements, as well as some amount of oxygen coming from the carbonized cellulose fibers (Figure S2. From the elemental mapping images (Figure 3b–e), we can observe a homogeneous distribution for all of the elements.

To quantify the carbon amount in CoMoS@C, TGA was performed from room temperature to 1000 °C under air atmosphere. The TGA curves of carbon fibers (Figure S3)

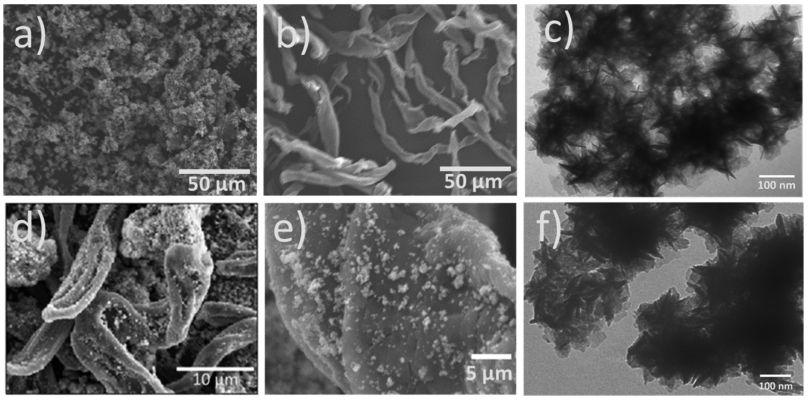

Figure 2. SEM of (a) bare-CoMoS, (b) cellulose fibers carbonized at 400 °C for 1 h, (d) CoMoS@C, and (e) CoMoS@C at higher magnification. TEM of (c) bare-CoMoS and (f) CoMoS@C.

DOI: 10.1021/acsomega.8b00654
ACS Omega 2018, 3, 10243−10249

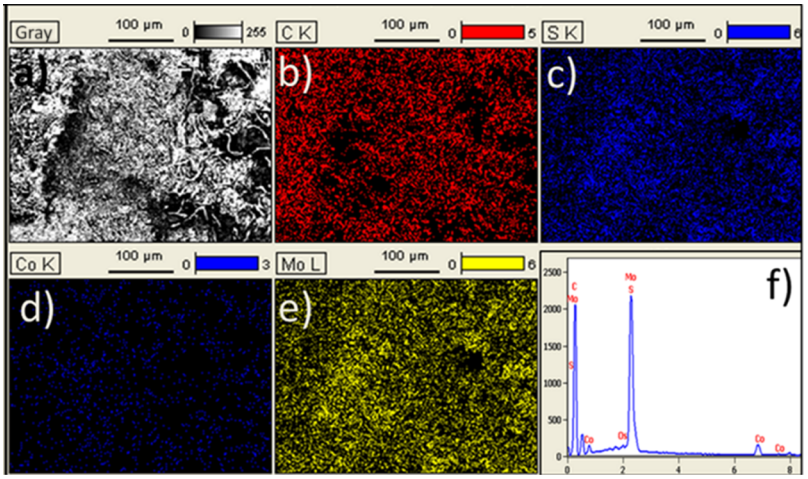

Figure 3. (a) SEM image of the selected area for sample CoMoS@C, (b–e) elemental mapping images of C, S, Co, and Mo. (f) EDS spectrum of CoMoS@C.

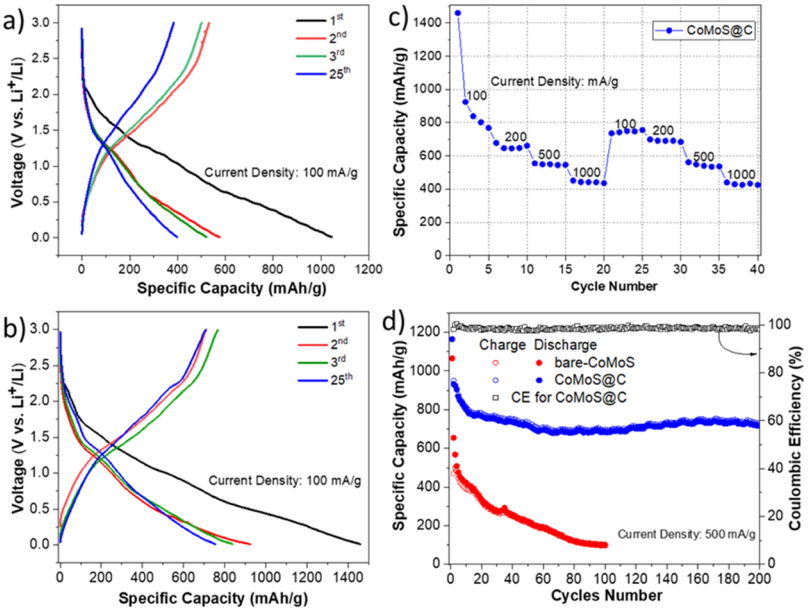

Figure 4. Charge/discharge voltage profiles at a current rate of 100 mA g^{-1} for (a) bare-CoMoS and (b) CoMoS@C. (c) Rate capability of CoMoS@C from 0.1 to 1 Ag^{-1}. (d) Cycling performance of CoMoS and CoMoS@C at a current rate of 500 mA/g and Coulombic efficiency (CE) for CoMoS@C.

showed a large reduction of weight from 100 to 8% starting from ∼350 °C up until 550 °C. Afterward, the sample weight kept nearly constant up until 1000 °C. The TGA results from CoMoS@C shows a weight reduction starting at ∼350 °C, this closely matches the weight loss of the carbon fibers. The CoMoS@C sample plateau at 550 °C with 72% leftover weight was caused by the conversion of carbon to CO_2. At temperatures greater than 550 °C, the oxidation of organic materials, Mo and Co, took place. Additionally, we can see that the weight drop from ∼400 to 500 °C is absent for bare-CoMoS. Therefore, the carbon content in sample CoMoS@C is estimated to be ∼28%.

The electrochemical performance of CoMoS@C was first evaluated by testing the charge/discharge galvanostatic measurements. Figure 4a displays the 1st, 2nd, 3rd, and 25th cycles at a current density of 100 mA/g between 0.01 and 3 V versus Li^+/Li for CoMoS@C sample. For comparison, we also present the charge/discharge results for bare-CoMoS under the same electrochemical conditions (Figure 4a). The discharge capacities for bare-CoMoS were 1043, 575, 519, and 396 mA h/g, respectively. By contrast, CoMoS@C (Figure 4b) showed significantly higher specific capacities of 1461, 925, 839, and 756 mA h/g, respectively. We also investigated the cycling performance of CoMoS@C for 200 cycles at a current rate of 500 mA/g (Figure 4d). CoMoS@C showed an initial high specific capacity of 1165 mA h/g and retained a high specific capacity value of ∼715 mA h/g and a CE above 97% after 200 cycles. In contrast, bare-CoMoS maintained a low specific capacity of ∼102 mA h/g after 100 cycles. The CoMoS@C composite kept a discharge capacity of ∼425 mA h/g (Figure 4c) when discharged at different rates (100, 200, 500, and 1000 mA/g) after 40 cycles.

To study the influence of the carbonized fibers in the cycling performance of CoMoS@C, an electrode of carbonized fibers was subjected to charge and discharge measurements for several cycles at a rate of 100 mA/g (Figure S4a,c). The carbon

DOI: 10.1021/acsomega.8b00654
ACS Omega 2018, 3, 10243−10249

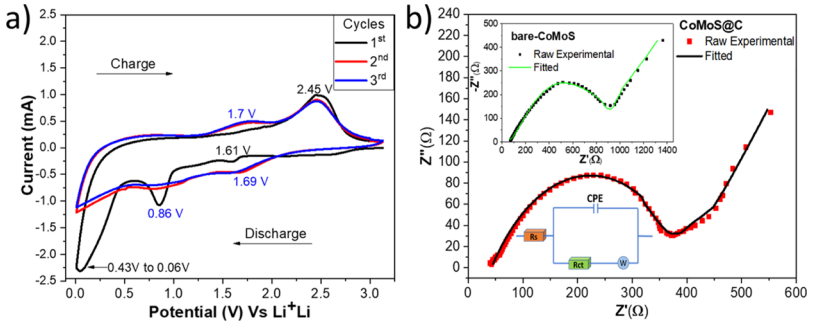

Figure 5. (a) CV and (b) Nyquist plots for CoMoS@C (inset: bare-CoMoS).

fiber material showed only one discharge and does not have the ability of recharging, probably due to the low carbonization temperature. Therefore, the superior electrochemical performance of the CoMoS@C electrode is due to the synergistic effect of CoMoS and the carbonized fibers. CoMoS contributes to the high specific capacity value, and the carbon fibers stabilize the cycling performance of the electrode. Carbon fibers improved the electrical conductivity (as is shown latter in the Nyquist plots, Figure 5b) as well as buffering the electrode volume changes and preventing the electrode material from pulverization, as reported previously in other publications.[37,38]

To further explore the electrochemical reactions of CoMoS@C and bare-CoMoS electrodes, CV measurements were performed for the first three cycles, and the results are shown in Figures 5a and S5b, respectively. The first cathodic scan for sample CoMoS@C presents three peaks at 1.61, 0.86 V, and another that ranges from ∼0.43 to ∼0.06 V. For the first anodic scan, only one big peak at ∼2.45 V is shown. In the following cycles, the cathodic peak in the range of ∼0.43 to 0.06 V disappears, the peak at 0.86 V stays at the same voltage position but the current decreased considerably, and the other peak becomes wider and slightly shifts from 1.61 to 1.69 V. Similarly, the peak at 2.45 V in the subsequent cycles for anodic scans stays in that potential and a new one appears at 1.7 V.

The peak at 0.86 V for the first cathodic scan can be attributed to the intercalation of Li ions into the lattice of $CoMoS_4$ (Li_xCoMoS_4), whereas the peak in the range of 0.43−0.06 V can be ascribed to the further reduction of Li_xCoMoS_4 into metallic Mo and Co embedded into a LiS_2 matrix and also to the formation of a gel-like polymer, resulting from the irreversible electrolyte degradation [also called the solid electrolyte interface (SEI)] in the first discharge, as is reported by a similar study[25] and other publications related to the intercalation of Li ions (lithiation) into molybdenum and cobalt sulfides.[6,12,39−43] In the second and third cathodic scans, the peak at 1.69 V can be assigned to the intercalation of Li ions into cobalt and molybdenum sulfides.[44,45] In addition, the peak in the range of 0.43−0.06 V disappears. This fact coupled with the big reduction in capacity from the first to the second discharge (charge/discharge curves, Figure 5b) confirms the irreversibility of the SEI formation. In contrast, the peaks at 1.7 and 2.45 V in the first anodic scan, as suggested by some studies, correspond to the conversion reaction of Mo and Co as well as LiS_2 to form molybdenum sulfide and cobalt sulfides,[25,45] whereas other studies allude that this latter peak (2.45 V) corresponds to the formation of LiS_2 to S_8^{-2}.[46]

In the subsequent cycles (CoMoS@C), the CV curves almost overlap each other, indicating good reversibility of the electrode. On the other hand, for sample bare-CoMoS (Figure S5b), the redox peak intensity significantly decreases over cycling, indicating poor cycling performance. This result implies that the carbon matrix stabilizes the cycling performance for CoMoS@C electrode as is demonstrated by other studies which used cobalt sulfide and molybdenum sulfide with and without carbon addition.[12,41,42,47,48]

To have a better understanding of the resistive behavior, electrochemical impedance spectroscopy (EIS) was conducted for bare-CoMoS, CoMoS@C (Figure 5b), and carbonized fibers (Figure S5a). Figure 5b shows the raw experimental and fitted Nyquist plots for CoMoS@C and CoMoS (inset of Figure 5b) as well as the equivalent circuit used for fitting the plots. The EIS curves for the three electrode materials are composed of a depressed semicircle in the high−medium frequency region and a straight line in the low-frequency region. The high−medium frequency semicircle is composed of R_s (Ohm resistance of the battery) and R_{ct} (charge-transfer resistance). The inclined line represents the Warburg impedance (W) caused by the Li ions diffusion. According to the equivalent circuit, the values for CoMoS and CoMoS@C are 72 and 40 Ω, respectively, and 65 Ω for carbonized fibers. The charge-transfer resistance (R_{ct}) for CoMoS@C is 327 Ω, 827 Ω for CoMoS, and 596 Ω for carbonized fibers. Therefore, the CoMoS@C electrode possesses the lowest charge-transfer resistance.

3. CONCLUSIONS

In summary, CoMoS@C composite was fabricated by the combination of CoMoS synthesized by hydrothermal method and cellulose fibers carbonized at 400 °C for 1 h. This composite shows significantly improved electrochemical performance when compared to bare-CoMoS. The carbonized bimetallic composite, CoMoS@C, retained a high specific discharge capacity of 715 mA h/g with a CE greater than 97% after 200 cycles at a current rate of 500 mA/g. The high specific discharge capacity and superior cycling stability can be accredited to the synergistic effect between the CoMoS and carbonized cellulose fibers. The use of biomass-derived carbon may offer an easy and cost-effective strategy to improve the electrochemical performance of metal and bimetallic sulfides and other metallic compounds.

4. EXPERIMENTAL SECTION

4.1. Synthesis of CoMoS. The synthesis of CoMoS (cobalt−molybdenum sulfide) was carried out by hydrothermal method in a high-pressure reactor (Par model 4540). The first step consisted the synthesis of ammonium thiomolybdate (ATM) that was synthesized following the

DOI: 10.1021/acsomega.8b00654
ACS Omega 2018, 3, 10243−10249

improved method by Alonso et al.[35] Next, ATM (19.2 mmol) was dispersed in a minimum amount of deionized water under constant stirring, followed by the addition of an equivalent molar amount (19.2 mmol) of NTA (nitriloacetic acid, Sigma-Aldrich) to this dispersion under stirring. Separately, 13.5 mmol of $CoNO_3 \cdot 6H_2O$ (Sigma-Aldrich) was dissolved in a minimum amount of deionized water and added to the ATM/NTA mixture. The reaction mixture was transferred to the reactor vessel and heated to 300 °C for 2 h. It is important to mention that the pressure inside the reactor increased to 1200 PSI when the reaction reached 300 °C.

4.2. Synthesis of CoMoS@C. First, 100 mg of CoMoS and 57 mg of medium-size cellulose fibers (cotton linters from Sigma-Aldrich) were placed in a vial and agitated for 5 min at 3000 rpm in a vortex machine. This mixture was placed in a ceramic boat, introduced into a tubular furnace (MTI Corporation, GSL-1100X-LD), and heated at 400 °C for 1 h at a heating rate of 5 °C/min under argon atmosphere. This sample was referred as CoMoS@C. For comparison purposes, CoMoS by itself was thermally treated under the same conditions and labeled as bare-CoMoS.

4.3. Characterization. XRD measurements were performed on a D8 diffractometer from Bruker Instruments (Cu Kα radiation, λ = 0.154 nm) with a scan rate of two degree/min. SEM and EDS images were obtained by using a Hitachi S-4800 machine. TEM images were acquired by a Hitachi H-7650 equipment. Image J software was used to measure the sizes of the particles and carbonized cellulose fibers from SEM images. TGA was conducted to quantify the carbon amount for CoMoS@C.

4.4. Electrochemical Measurements. The working electrodes were prepared by mixing the active material (CoMoS@C), acetylene black, and a binder composed of sodium carboxymethyl cellulose dissolved in deionized water (3 wt %) in a weight ratio percentage of 70:15:15, respectively. The obtained slurry was then coated onto a copper foil and dried overnight under vacuum at 100 °C. The electrodes were cut with a diameter of 1.3 cm using a precision disc cutter from MTI Corporation. The coin cells (CR 2032) were assembled inside of an Ar-filled glovebox with oxygen levels maintained below 0.1 ppm. Li foil was used as the counter/reference electrode, a ceramic-coated membrane (16 μm thick) from MTI Corporation was utilized as the separator (EQ-bsf-0016-500A), and the electrolyte employed was 1.0 M $LiPF_6$ in ethylene carbonate/dimethyl carbonate (1:1 in volume) from Sigma-Aldrich. The specific capacity was calculated based on the active material weight. The galvanostatic charge/discharge measurements were performed in an eight-channel battery analyzer (MTI Corporation) with a voltage window of 0.01−3 V. The EIS and CV studies were conducted in a CHI760D electrochemical workstation. EIS was measured in coin cells in a frequency range of 0.01−100 000 Hz at an ac amplitude of 0.05 V. The CV was evaluated in a three-electrode setup using an electrochemical cell (990-00343) from Gamry Instruments within the range of 3.0−0.01 V at a scan rate of 0.01 V.

■ ASSOCIATED CONTENT

Supporting Information

The Supporting Information is available free of charge on the ACS Publications website at DOI: 10.1021/acsomega.8b00654.

XRD patterns of carbonized cellulose fibers; EDS spectrum of carbonized cellulose fibers; TGA for samples CoMoS@C, bare-CoMoS and carbonized cellulose fibers; charging and discharging plots for carbonized cellulose fibers; Nyquist plots for carbon fibers; and CV curves for bare-CoMoS (PDF)

■ AUTHOR INFORMATION

Corresponding Author

*E-mail: jcnoveron@utep.edu.

ORCID

Noemi Dominguez: 0000-0001-7124-2603

Luis A. Barrera: 0000-0003-4378-4397

Notes

The authors declare no competing financial interest.

■ ACKNOWLEDGMENTS

Financial support from the NSF PREM DMR-1205302, the NSF ERC on Nanotechnology-Enabled Water Treatment 1449500, the NSF CHE-0748913, the USDA 2014-38422-22078, and the Ralph & Kathleen Ponce de Leon Endowment at UTEP are gratefully acknowledged. The authors thank Dr. Dino Villagran and Ivan Cervantes for their help with CV and EIS. The authors gratefully acknowledge the CONACYT for the financial support.

■ REFERENCES

(1) Vetter, M.; Lux, S. Rechargeable Batteries with Special Reference to Lithium-Ion Batteries. *Storing Energy* **2016**, 205−225.

(2) Aurbach, D.; Markovsky, B.; Weissman, I.; Levi, E.; Ein-Eli, Y. On the Correlation between Surface Chemistry and Performance of Graphite Negative Electrodes for Li Ion Batteries. *Electrochim. Acta* **1999**, *45*, 67−86.

(3) Xu, L.; Hu, Y.; Zhang, H.; Jiang, H.; Li, C. Confined Synthesis of FeS2 Nanoparticles Encapsulated in Carbon Nanotube Hybrids for Ultrastable Lithium-Ion Batteries. *ACS Sustainable Chem. Eng.* **2016**, *4*, 4251−4255.

(4) Wang, C.; Wan, W.; Huang, Y.; Chen, J.; Zhou, H. H.; Zhang, X. X. Hierarchical MoS2 nanosheet/active carbon fiber cloth as a binder-free and free-standing anode for lithium-ion batteries. *Nanoscale* **2014**, *6*, 5351−5358.

(5) Guo, J.; Li, F.; Sun, Y.; Zhang, X.; Tang, L. Graphene-Encapsulated Cobalt Sulfides Nanocages with Excellent Anode Performances for Lithium Ion Batteries. *Electrochim. Acta* **2015**, *167*, 32−38.

(6) Wang, Q.; Li, J. Facilitated Lithium Storage in MoS2Overlayers Supported on Coaxial Carbon Nanotubes. *J. Phys. Chem. C* **2007**, *111*, 1675−1682.

(7) Lin, Y.-C.; Zhang, W.; Huang, J.-K.; Liu, K.-K.; Lee, Y.-H.; Liang, C.-T.; Chu, C.-W.; Li, L.-J. Wafer-Scale MoS2 Thin Layers Prepared by MoO3 Sulfurization. *Nanoscale* **2012**, *4*, 6637.

(8) Zhang, X.; Li, X.; Liang, J.; Zhu, Y.; Qian, Y. Synthesis of MoS2 @C Nanotubes Via the Kirkendall Effect with Enhanced Electrochemical Performance for Lithium Ion and Sodium Ion Batteries. *Small* **2016**, *12*, 2484−2491.

(9) Geng, H.; Yang, J.; Dai, Z.; Zhang, Y.; Zheng, Y.; Yu, H.; Wang, H.; Luo, Z.; Guo, Y.; Zhang, Y.; et al. Co9S8/MoS2Yolk−Shell Spheres for Advanced Li/Na Storage. *Small* **2017**, *13*, 1603490.

(10) Wang, Q.; Jiao, L.; Han, Y.; Du, H.; Peng, W.; Huan, Q.; Song, D.; Si, Y.; Wang, Y.; Yuan, H. CoS2 Hollow Spheres: Fabrication and Their Application in Lithium-Ion Batteries. *J. Phys. Chem. C* **2011**, *115*, 8300−8304.

(11) Wang, J.; Ng, S. H.; Wang, G. X.; Chen, J.; Zhao, L.; Chen, Y.; Liu, H. K. Synthesis and Characterization of Nanosize Cobalt Sulfide

DOI: 10.1021/acsomega.8b00654
ACS Omega 2018, 3, 10243−10249

for Rechargeable Lithium Batteries. *J. Power Sources* **2006**, *159*, 287−290.
(12) Huang, Z. X.; Wang, Y.; Wong, J. I.; Shi, W. H.; Yang, H. Y. Synthesis of Self-Assembled Cobalt Sulphide Coated Carbon Nanotube and Its Superior Electrochemical Performance as Anodes for Li-Ion Batteries. *Electrochim. Acta* **2015**, *167*, 388−395.
(13) Zhou, Y.; Yan, D.; Xu, H.; Liu, S.; Yang, J.; Qian, Y. Multiwalled carbon nanotube@a-C@Co9S8nanocomposites: a high-capacity and long-life anode material for advanced lithium ion batteries. *Nanoscale* **2015**, *7*, 3520−3525.
(14) Gu, Y.; Xu, Y.; Wang, Y. Graphene-Wrapped CoS Nanoparticles for High-Capacity Lithium-Ion Storage. *ACS Appl. Mater. Interfaces* **2013**, *5*, 801−806.
(15) Lao, M.; Zhao, G.; Li, X.; Chen, Y.; Dou, S. X.; Sun, W. Homogeneous Sulfur−Cobalt Sulfide Nanocomposites as Lithium−Sulfur Battery Cathodes with Enhanced Reaction Kinetics. *ACS Appl. Energy Mater.* **2017**, *1*, 167.
(16) Xu, H.; Manthiram, A. Hollow Cobalt Sulfide Polyhedra-Enabled Long-Life, High Areal-Capacity Lithium-Sulfur Batteries. *Nano Energy* **2017**, *33*, 124−129.
(17) Yu, L.; Yang, J. F.; Lou, X. W. D. Formation of CoS2 Nanobubble Hollow Prisms for Highly Reversible Lithium Storage. *Angew. Chem., Int. Ed.* **2016**, *55*, 13422−13426.
(18) Wang, W.; Li, L.; Tan, S.; Wu, K.; Zhu, G.; Liu, Y.; Xu, Y.; Yang, Y. Preparation of NiS 2 //MoS 2 catalysts by two-step hydrothermal method and their enhanced activity for hydrodeoxygenation of p -cresol. *Fuel* **2016**, *179*, 1−9.
(19) Bui, V. N.; Laurenti, D.; Delichère, P.; Geantet, C. Hydrodeoxygenation of guaiacol. *Appl. Catal., B* **2011**, *101*, 246−255.
(20) Yoosuk, B.; Kim, J. H.; Song, C.; Ngamcharussrivichai, C.; Prasassarakich, P. Highly active MoS2, CoMoS2 and NiMoS2 unsupported catalysts prepared by hydrothermal synthesis for hydrodesulfurization of 4,6-dimethyldibenzothiophene. *Catal. Today* **2008**, *130*, 14−23.
(21) Shen, X.; Xia, X.; Ye, W.; Du, Y.; Wang, C. Hexagram-like CoS-MoS2 Composites with Enhanced Activity for Hydrogen Evolution Reaction. *J. Solid State Electrochem.* **2017**, *21*, 409−417.
(22) Wu, Z.; Guo, J.; Wang, J.; Liu, R.; Xiao, W.; Xuan, C.; Xia, K.; Wang, D. Hierarchically Porous Electrocatalyst with Vertically Aligned Defect-Rich CoMoS Nanosheets for the Hydrogen Evolution Reaction in an Alkaline Medium. *ACS Appl. Mater. Interfaces* **2017**, *9*, 5288−5294.
(23) Guo, Y.; Gan, L.; Shang, C.; Wang, E.; Wang, J. A Cake-Style CoS@MoS/RGO Hybrid Catalyst for Efficient Hydrogen Evolution. *Adv. Funct. Mater.* **2017**, *27*, 1602699.
(24) Zhang, H.; Li, Y.; Xu, T.; Wang, J.; Huo, Z.; Wan, P.; Sun, X. Amorphous Co-doped MoS2 nanosheet coated metallic CoS2 nanocubes as an excellent electrocatalyst for hydrogen evolution. *J. Mater. Chem. A* **2015**, *3*, 15020−15023.
(25) Lu, Y.; Fong, E. Biomass-Mediated Synthesis of Carbon-Supported Nanostructured Metal Sulfides for Ultra-High Performance Lithium-Ion Batteries. *J. Mater. Chem. A* **2016**, *4*, 2738−2745.
(26) Wang, J.; Liu, J.; Yang, H.; Chao, D.; Yan, J.; Savilov, S. V.; Lin, J.; Shen, Z. X. MoS 2 nanosheets decorated Ni 3 S 2 @MoS 2 coaxial nanofibers: Constructing an ideal heterostructure for enhanced Na-ion storage. *Nano Energy* **2016**, *20*, 1−10.
(27) Park, J.-S.; Kang, Y. C. Multicomponent (Mo, Ni) Metal Sulfide and Selenide Microspheres with Empty Nanovoids as Anode Materials for Na-Ion Batteries. *J. Mater. Chem. A* **2017**, *5*, 8616−8623.
(28) Teng, Y.; Zhao, H.; Zhang, Z.; Li, Z.; Xia, Q.; Zhang, Y.; Zhao, L.; Du, X.; Du, Z.; Lv, P.; et al. MoS2 Nanosheets Vertically Grown on Graphene Sheets for Lithium-Ion Battery Anodes. *ACS Nano* **2016**, *10*, 8526−8535.
(29) Zhao, B.; Wang, Z.; Gao, Y.; Chen, L.; Lu, M.; Jiao, Z.; Jiang, Y.; Ding, Y.; Cheng, L. Hydrothermal synthesis of layer-controlled MoS 2 /graphene composite aerogels for lithium-ion battery anode materials. *Appl. Surf. Sci.* **2016**, *390*, 209−215.
(30) Lv, X.; Deng, J.; Wang, B.; Zhong, J.; Sham, T.-K.; Sun, X.; Sun, X. γ-Fe2O3@CNTs Anode Materials for Lithium Ion Batteries Investigated by Electron Energy Loss Spectroscopy. *Chem. Mater.* **2017**, *29*, 3499−3506.
(31) Yu, W.-J.; Zhang, L.; Hou, P.-X.; Li, F.; Liu, C.; Cheng, H.-M. High Reversible Lithium Storage Capacity and Structural Changes of Fe 2 O 3 Nanoparticles Confined inside Carbon Nanotubes. *Adv. Energy Mater.* **2015**, *6*, 1501755.
(32) Wu, F.; Huang, R.; Mu, D.; Wu, B.; Chen, Y. Controlled synthesis of graphitic carbon-encapsulated α-Fe2O3 nanocomposite via low-temperature catalytic graphitization of biomass and its lithium storage property. *Electrochim. Acta* **2016**, *187*, 508−516.
(33) Wu, J.; Zuo, L.; Song, Y.; Chen, Y.; Zhou, R.; Chen, S.; Wang, L. Preparation of biomass-derived hierarchically porous carbon/Co 3 O 4 nanocomposites as anode materials for lithium-ion batteries. *J. Alloys Compd.* **2016**, *656*, 745−752.
(34) Wen, T.; Wu, X.-L.; Zhang, S.; Wang, X.; Xu, A.-W. Core-Shell Carbon-Coated CuO Nanocomposites: A Highly Stable Electrode Material for Supercapacitors and Lithium-Ion Batteries. *Chem.—Asian J.* **2015**, *10*, 595−601.
(35) Alonso, G.; Yang, J.; Siadati, M. H.; Chianelli, R. R. Synthesis of Tetraalkylammonium Thiometallates in Aqueous Solution. *Inorg. Chim. Acta* **2001**, *325*, 193−197.
(36) Chateigner, D.; Chen, X.; Ciriotti, M.; Downs, R. T.; Gražulis, S.; Kaminsky, W.; Bail, A. Le.; Lutterotti, L.; Matsushita, Y.; Moeck, P.; et al. Crystallographic Open Database, http://www.crystallography.net/cod/.
(37) Wu, R.; Wang, D. P.; Rui, X.; Liu, B.; Zhou, K.; Law, A. W. K.; Yan, Q.; Wei, J.; Chen, Z. In-Situ Formation of Hollow Hybrids Composed of Cobalt Sulfides Embedded within Porous Carbon Polyhedra/carbon Nanotubes for High-Performance Lithium-Ion Batteries. *Adv. Mater.* **2015**, *27*, 3038−3044.
(38) Peng, S.; Han, X.; Li, L.; Zhu, Z.; Cheng, F.; Srinivansan, M.; Adams, S.; Ramakrishna, S. Unique Cobalt Sulfide/Reduced Graphene Oxide Composite as an Anode for Sodium-Ion Batteries with Superior Rate Capability and Long Cycling Stability. *Small* **2016**, *12*, 1359−1368.
(39) Li, H.; Li, W.; Ma, L.; Chen, W.; Wang, J. Electrochemical Lithiation/delithiation Performances of 3D Flowerlike MoS2 Powders Prepared by Ionic Liquid Assisted Hydrothermal Route. *J. Alloys Compd.* **2009**, *471*, 442−447.
(40) Hwang, H.; Kim, H.; Cho, J. MoS2Nanoplates Consisting of Disordered Graphene-like Layers for High Rate Lithium Battery Anode Materials. *Nano Lett.* **2011**, *11*, 4826−4830.
(41) Jin, R.; Liu, J.; Xu, Y.; Li, G.; Chen, G. Solvothermal synthesis and excellent electrochemical performance of polycrystalline rose-like Co9S8 hierarchical architectures. *J. Mater. Chem. A* **2013**, *1*, 7995−7999.
(42) Chang, K.; Chen, W. l-Cysteine-Assisted Synthesis of Layered MoS2/Graphene Composites with Excellent Electrochemical Performances for Lithium Ion Batteries. *ACS Nano* **2011**, *5*, 4720−4728.
(43) Du, G.; Guo, Z.; Wang, S.; Zeng, R.; Chen, Z.; Liu, H. Superior Stability and High Capacity of Restacked Molybdenum Disulfide as Anode Material for Lithium Ion Batteries. *Chem. Commun.* **2010**, *46*, 1106−1108.
(44) Guo, J.; Li, F.; Sun, Y.; Zhang, X.; Tang, L. Graphene-Encapsulated Cobalt Sulfides Nanocages with Excellent Anode Performances for Lithium Ion Batteries. *Electrochim. Acta* **2015**, *167*, 32−38.
(45) Shokhen, V.; Miroshnikov, Y.; Gershinsky, G.; Gotlib, N.; Stern, C.; Naveh, D.; Zitoun, D. On the Impact of Vertical Alignment of MoS2 for Efficient Lithium Storage. *Sci. Rep.* **2017**, *7*, 3280.
(46) Stephenson, T.; Li, Z.; Olsen, B.; Mitlin, D. Lithium ion battery applications of molybdenum disulfide (MoS2) nanocomposites. *Energy Environ. Sci.* **2014**, *7*, 209−231.
(47) Deng, Z.; Jiang, H.; Hu, Y.; Liu, Y.; Zhang, L.; Liu, H.; Li, C. 3D Ordered Macroporous MoS2 @C Nanostructure for Flexible Li-Ion Batteries. *Adv. Mater.* **2017**, *29*, 1603020.
(48) Kong, S.; Jin, Z.; Liu, H.; Wang, Y. Morphological Effect of Graphene Nanosheets on Ultrathin CoS Nanosheets and Their

DOI: 10.1021/acsomega.8b00654
ACS Omega 2018, 3, 10243−10249

Applications for High-Performance Li-Ion Batteries and Photocatalysis. *J. Phys. Chem. C* **2014**, *118*, 25355−25364.

DOI: 10.1021/acsomega.8b00654
ACS Omega 2018, 3, 10243−10249